TR－H－030

Morphological and acoustical analysis of the nasal and the paranasal cavities

Jianwu DANG　Kiyoshi HONDA
Hisayoshi SUZUKI

1993. 9. 24

ATR人間情報通信研究所

〒619-02 京都府相楽郡精華町光台2-2　☎07749-5-1011

ATR Human Information Processing Research Laboratories

2-2, Hikaridai, Seika-cho, Soraku-gun, Kyoto 619-02 Japan

Telephone: +81-7749-5-1011
Facsimile: +81-7749-5-1008

Morphological and acoustical analysis of the nasal and the paranasal cavities

Jianwu DANG, Kiyoshi HONDA

ATR Human Information Processing Research Laboratories
2-2 Hikaridai Seika-cho Soraku-gun Kyoto Japan, 619-02.

Hisayoshi SUZUKI

Faculty of engineering, Shizuoka University.
3-5-1 Jouhoku Hamamatsu, Japan 432.

This paper has been submitted for publication in the Journal of the Acoustical Society of America.

ABSTRACT

Morphological measurements of the nasal and paranasal cavities were measured to investigate on acoustic properties of the human nasal tract. The magnetic resonance imaging (MRI) technique was used to measure the three-dimensional geometry of the vocal tract. The area function of the nasal tract was calculated for seven subjects using natural breathing. The entire vocal tract was measured for five subjects during sustained production of nasal consonants. A marked morphological difference was observed between our data and previously published data particularly in the middle portion of the nasal tract. Previous data derived from cadaver specimens indicated a wide cavity in the middle portion possibly due to absent or dehydrated mucous membrane, while our data showed narrow passages caused by thick mucosa. It has been confirmed by experiment that the wide cavity is reproducible by applying an adrenaline-like agent inside the nose. Transfer functions of the vocal tract and the nasal tract were calculated from measured data, and compared to spectra of real speech signals recorded subsequent to the MRI experiment. The results indicate that asymmetry between the two nasal passages can cause extra pole-zero pairs, and suggest that the paranasal cavities play an important role in shaping spectral characteristics of human nasal sounds.

PACS number: 43.70.Aj, 43.70.Bk.

INTRODUCTION

The previously available data of nasal tract shape were measured from a cadaver specimen of the skull by House, et al. (1956), and from a plastic mold of the nasal tract by Fant (1960). It has been noted, however, that these data do not provide realistic predictions on the properties of real nasal sounds (Fujimura, & Lindqvst, 1971; Takeuchi, Kasuya, & Kido, 1977; Maeda, 1982). The value of the lowest resonance frequency of the nasal tract is too high in simulations based on these previous data (Maeda, 1982). The results of sweep-tone experiments (Fujimura, & Lindqvst, 1971; Lindqvst-Gauffin, & Sundberg, 1976) have shown that nasal pole-zero pairs appeared near and often below the first formant peak, especially for low vowels, even though the pole-zero pair predicted from traditional models of the nasal tract without the paranasal cavities is located above the first shifted vowel formant peak. These facts have suggested that the acoustic effect of the "subsidiary cavities" within the nose and/or of the asymmetry of the nasal passages may play an important role in shaping appropriate nasal spectra (Fujimura, & Lindqvst, 1964; Fant, 1980; Maeda, 1982). Takeuchi, et al. (1977) estimated the volumes of the paranasal sinuses and their ostiums, which are the conduits to the nasal tract, from a cadaver specimen of the skull, and discussed the resonance properties of the nasal cavity when the sinuses were taken into account. Maeda (1982) estimated the volume of the paranasal cavity and the area and length of its ostium by means of an analysis-by-synthesis procedure, where he treated the paranasal cavities as a single sinus cavity. Masuda (1992) measured the maxillary sinus by dissecting more than 20 skulls, and gave anatomical data of the maxillary sinus. Dang, et al. (1993) investigated the variation of nasal tract shape with nasal mucosa when the nasal tract was treated with

and without an adrenaline-like agent. It is known that there is a considerably thick layer of the mucosa covering the inside surface of the nasal cavity for the living, which would reduce the volume of the nasal cavity. Purposes of the present research are to measure morphological details of the nasal cavity for the living, and to investigate the relationship between nasal tract shape and its acoustic characteristics.

Magnetic resonance imaging (MRI) system is a powerful tool for morphological measurement of complicated shape of the nasal cavity. Baer, et al. (1991) and Moor (1992) used the MRI technique to measure oral tract shape during sustained production of vowel sounds, and described the method in detail in their papers. In the present research, we used MRI equipment to measure the shape of the nasal tract and the paranasal sinuses. To investigate the acoustical relationship of the nasal cavity to the nasal sound, we also measured the entire vocal tract, which includes the pharyngeal, oral and nasal cavities, during sustained production of nasal consonants. Since MRI equipments generate large periodical scan sounds, simultaneous recordings of clean speech sounds cannot be expected. Therefore, speech signals were recorded soon after MRI scan, while the subjects were instructed to keep the same posture of articulatory organs as that of during MRI scanning. The nasal transfer function was calculated from the MRI data, and was compared with that of real speech sounds.

I. EXPERIMENTAL PROCEDURES

A. MRI equipment and scanning parameters

We used a Shimadzu Magnetic Resonance Computer Tomograph, SMT-100GUX, which has a static magnetic field density of 1.0 Tesla to record three-dimensional images of the nasal and oral tracts. In the present study, we performed two experiments. Experiment 1 was to measure nasal cavity shape with a high

resolution but a small field of view. Experiment 2 was to measure the entire vocal tract, which included the pharyngeal, oral and nasal cavities, with a large field of view and somewhat reduced resolution. The subjects for Experiment 1 were six males and one female aged between 26 and 43 years old. Five subjects out of them served for Experiment 2. The spin echo pulse sequence was used for the experiments. The relaxation times (TR) were 1200 msec for Experiment 1 and 930 msec for Experiment 2. The excitation time (TE) was 18 msec for both experiments. Each image slice was the average of two excitations. The slice thickness was 0.3 cm for all images, with neither a gap nor an overlap between slices. In order to view detailed structure of the nasal cavity, slices were oriented along the coronal plane for Experiment 1. Similarly, slices were oriented along the sagittal plane for Experiment 2 to observe the shape of vocal tract easily.

In Experiment 1, images of the nasal cavity were obtained from each subject's rest state, most likely with collapsed oral cavity. Each coronal series consisted of 39 images, and covered an anterior-posterior span of 11.7 cm. The 25 cm × 25 cm field of view of each image was digitally represented by 256 × 256 pixel matrix so that spatial resolution of 0.0977 cm × 0.0977 cm × 0.3 cm per voxel was obtained. The scan time for the series of images was approximately 8 minutes.

In Experiment 2, images of the entire vocal tract were obtained in the sagittal orientation. For those measurements, subjects were instructed to sustain production of nasal consonants during MRI scanning. Speech materials for nasals were /m/ and /n/. Each image series consisted of 30 slices, and covered a right-to-left span of 9.0 cm. The 30 cm × 30 cm field of view of each image was digitally represented by 256 × 256 pixel matrix so that spatial resolution was 0.117 cm × 0.117 cm × 0.3 cm per voxel. It needed about 5 minutes to take a series of MRI images.

B. Analysis of MRI images

Most previous measurements of the vocal tract have been concerned with cross-sectional areas of the airway. However, it is not appropriate to infer the acoustical characteristics of the nasal cavity from the cross-sectional area of the nasal tract alone, because its complicated morphological composition can potentially affect the propagation of sound wave. In our analysis of cross-sectional areas of the nasal tract, we also measured cross-sectional circumferences of the nasal tract as an index of the morphological complexity. In addition to the main nasal tract geometry, we determined the volume and the position of the paranasal cavities, and measured the ostiums from the paranasal cavities to the main nasal passages. The measurements were performed on a PC (Macintosh) with the Photoshop image analysis software. Image analysis involved edge detection of the air-tissue boundary of the nasal cavity and shape extraction of the air-passage. The software was used to automatically detect the air-tissue boundary, after the desired threshold value for the boundary had been specified. The detected boundaries were manually corrected in some locations where the airways are too narrow for the software to automatically draw an accurate boundary line. The area and circumference of airways in a section were obtained by counting the number of the pixels inside and on the fringe of the airways, respectively.

Figure 1 shows examples of coronal MRI slices of the nasal cavity from Experiment 1. The brightness of the image in our scan method roughly corresponds to the amount of water in the materials, being lower in air and bone, and higher in mucosa and muscle. Figure 2 plots sectional shapes of the nasal cavity and the paranasal cavities, which were extracted from the slices of Figure 1. Figure 2 (a) is the image at 3 cm from the posterior wall of the middle pharynx, showing the section of the sphenoidal sinus (S. S.) on the top, and the section of the nasal passage (N. P.) on the bottom, where the nasal tract is a single tube. Figure 2 (b) is the image at 5.4 cm from the

posterior wall of the pharynx, demonstrating a section of the ethomoidal sinus (E. S.) on the top, and a section of the maxillary sinus (M. S.) on both sides. A section of the nasal tract is shown in the middle of the figure where it separates into two passages exhibiting very complicated thin airways. Figure 2 (c) is the image at 8.4 cm from the posterior wall of the pharynx. The upper part is a section of the frontal sinus (F. S.), and the lower part is a section of the nasal tract showing two flat tubes. The morphological variation in different parts of the nasal tract makes it difficult to obtain meaningful numerical data of nasal tract shape. For the sake of reducing the effect of the variation, we divide the nasal tract into posterior, middle and anterior portions. As Figure 2 describes, the sectional plane of the nasal tract is a circle-like shape for the posterior portion, a butterfly-like shape for the middle portion, and two parallel tubes for the anterior portion. In the following, we describe morphological differences of the nasal tract according to these three divisions when necessary.

II. RECONSTRUCTING OF THE NASAL AND PARANASAL CAVITIES

A. Reconstructing a three-dimensional image

A three-dimensional reconstruction of the nasal cavity and the paranasal cavities was made from extracted data of their sectional shapes as described in Section 2.2, by means of a software named "Voxel View" on an IRIS workstation. A projection of a reconstructed 3D image of the nasal tract is shown in Figure 3. The nostrils are on the right hand side in Figure 3, and the glottis is in the bottom of the left hand side. Figure 4 (a) shows three sagittal slices of the right side of the nasal cavity in 0.3 cm intervals. Figure 4 (b) shows three slices in transverse planes, which were located on the levels of the inferior meatus, the middle meatus and the superior meatus, respectively. The coronal slices of the 3D image have been

shown in Figure 2. These figures depict the complexity of the nasal cavity shape from several different views.

B. Obtaining cross-sectional slices along the nasal tract

When sound wave propagating inside a tube is considered as a plane wave, the acoustical property of the tube is mainly dependent on its area function, which can be described by a series of cross-sectional areas perpendicular to the midline with the same interval between them. The area function is easy to measure if the cross-sectional areas of the vocal tract are parallel to transverse or coronal planes. Unfortunately, the cross-sectional areas are not always like that, because there are different curvatures in different portions of the vocal tract. The MRI equipment we used is capable of multiangle-scan, which is a method for picturing a series of images with arbitrary angles. However, imaging planes have to be programmed in prior to scan and this procedure takes considerable time and efforts, and often results in inaccurate positioning of scan planes. Fortunately, the previously mentioned VoxelView software is able to compute the image of slices in any specified angle and position from a reconstructed 3D image. This function is suitable for measuring cross-sectional images that are perpendicular to the midline along the vocal tract. Figure 5 shows an example of the midsagittal plane with a series of lines which are projections of the planes to specify the cross-sectional images, where the posture of articulatory organs is for uttering nasal consonant /m/. Cross-sectional areas of the vocal tract were measured by this technique in the following analysis.

The procedure of obtaining the axial slices, in this example, is hand-tracing a midline of the oral and nasal tracts on the midsagittal image, followed by drawing of a series of lines perpendicular to the midline. Each line has an interval of 0.6 cm along the midline, and shows the angle and position of the associated axial plane. The planes were sliced from the reconstructed 3D image according to the lines,

and were then used to calculate areas and circumferences of the vocal tract airway.

In Experiment 1, MRI slices near the nostrils and the velopharyngeal port were not perpendicular to the midline of the nasal tract. Using the method mentioned above, we sliced a reconstructed 3D image of coronal slices into the axial sectional planes, and obtained cross-sectional areas in those portions. The cross-sectional areas and circumferences in middle portion of the nasal tract were calculated from raw MRI slices.

In Experiment 2, we measured cross-sectional areas of the pharyngeal and oral cavities. For the nasal tract, only the posterior portion of the nasal tract was measured, because areas within that region are affected by velum positions dependent on nasal context. The cross-sectional areas and circumferences of the anterior and middle portions of the nasal tract were measured from Experiment 1, which are more accurate than that from Experiment 2.

III. EXPERIMENTAL RESULTS AND MORPHOLOGICAL ANALYSIS

A. Area function of the nasal tract

In Experiment 1, cross-sectional areas of the nasal tract were obtained by using the method described in Section 3.2. The resultant area functions are shown in Figure 6 for four subjects. Notice that area is greater in the portion behind the branch of two nasal passages than in the middle and the anterior portions of the nasal tract, and that there is a considerable asymmetry between the left and right passages that bifurcate at about the 10th section from the velopharyngeal port. The data in Figure 6 show that the area function of the nasal tract varies widely from one subject to another.

Numerical measurements of the nasal tract for the four subjects are listed in Table I. The average length of the nasal tract is 11.6 cm, its standard deviation (Std.) is 0.13 cm, and its coefficient of variation (C. V.), which is defined as a ratio of standard deviation to

average of the length, is about 1%. Average volume is 25.5 cm^3, and its standard deviation and coefficient of variation are about 9.1 cm^3 and 36%, respectively. The numerical data show that individual difference in the volume of the nasal tract is much greater than that in the length.

In Table I, we also show the data when the nasal tract was divided into three portions as described in Section 2.2. Their average lengths are 3.9 cm for the posterior portion, 4.4 cm for the middle portion and 3.4 cm for the anterior portion, respectively. It is observed that C. V. varies considerably with the portions of the nasal tract. C. V. for length is less than 10% in all the three portions, and C. V. for volume is greater than 20%. The middle portion of the nasal tract has the largest C. V. in volume, which is 37.4%. It indicates that individual difference of volume is greater in the middle portion than in the other portions.

There is a notable difference between our nasal tract area function and published data (House, & Stevens, 1956, Fant, 1960), especially in the middle portion of the nasal tract. It has been mentioned that the previous data were measured from cadaver specimens or a plastic mold where the mucous membrane is absent or dehydrated. The difference between previous data and our own is demonstrated by comparing, for example, Fant's data (Fant, 1960) and one of our subjects shown in Figure 7 (a) and (b) respectively. Our data is from Subject 2 who had neither a cold nor a stuffy nose during this MRI scanning. To clarify whether the difference is caused by the morphological difference or by a variation in the nasal mucosa, we sprayed adrenaline-like agent, which is a kind of vasoconstrictor agent for a stuffy nose, into the nose of the subject. The area function of the nasal tract treated with the nasal spray is plotted in Figure 7 (c). After the treatment, the area function is quite different from that without the treatment shown in Figure 7 (b), where volume of the mucosa was greatly reduced. The cross-sectional area treated with the nasal decongestant is about twice as large as the normal area in

the middle portion. For the other subjects, similarly, the area treated with adrenaline is as about twice as that before the treatment. It implies that about a half of cross-sectional area in the middle tract is occupied by compressible nasal mucosa.

After the nasal tract was treated with the nasal spray, its area function becomes similar to that of Fant's data. This indicates that the difference is due primarily to the presence of the nasal mucosa of living condition. Our data should therefore represent the acoustic properties of the nasal tract more realistically than previous models, because our area function gives a better representation of nasal tract geometry.

B. Cross-sectional circumference of the nasal tract

Cross-sectional circumferences of the nasal tract were obtained by counting the number of the pixels on the air-tissue boundary of the cross-sectional area. Measured cross-sectional circumferences are plotted in Figure 8 for the four subjects. A pertinent characteristic of the data is that the circumferences of the middle portion of the nasal tract are much larger than those of the portion behind the branch of the left and right passages, even though the middle portions have smaller cross-sectional areas (see Figure 6). The surface of the posterior portion has a smaller C. V. than the other portions (see Table I). The average circumferences are 5.8 cm for the posterior portion, 20.2 cm for the middle portion, and 8.6 cm for the anterior portion. However, the areas do not change much. This fact shows that the middle portion has a much more complicated shape than the other portions.

In order to describe the complexity of nasal tract shape, Fant (1960) proposed a shape factor of the nasal cavity as Formula (1) below, and suggested its value is of the order of 3:

$$Sf = \frac{S}{\sqrt{4\pi A}} \qquad (1)$$

where S_f is the shape factor, S is a cross-sectional circumference, and A is a cross-sectional area of the nasal tract. We use the same formula to calculate the shape factor of every section for four subjects. The results are plotted in Figure 9. In the result, the shape factor is of the order of 4 for the middle portion, 1 for the posterior portion, and 2 for the anterior portion. Length of those portions is about 4.5 cm, 3.5 cm and 3.6 cm, respectively.

From Figure 6 and Figure 8, it is known that both of the area and circumference of the nasal tract have a strong asymmetry. To describe the asymmetry quantitatively, we define an asymmetry coefficient of nasal tract shape in Formula (2):

$$S_{si} = \left| \frac{Sf^{l}_{i} - Sf^{r}_{i}}{Sf^{l}_{i} + Sf^{r}_{i}} \right| \qquad (2)$$

where S_{si} is shape asymmetry coefficient of the nasal tract, i is the number of sections. Sf^{l}_{i} and Sf^{r}_{i} are left and right shape factors of the nasal tract, which are described in Formula (1).

It is known that the reflection coefficient described in Formula (3) is related to acoustic characteristics of a sound tube directly. So we use the reflection coefficient to defined an asymmetry coefficient of area function in Formula (4):

$$r = \frac{A_{i+1} - A_i}{A_{i+1} + A_i} \qquad (3)$$

$$S_{ai} = \left| r^{r}_{i} - r^{l}_{i} \right| \qquad (4)$$

where r is the reflection coefficient and S_{ai} is the asymmetry coefficient of area function of the nasal tract. A_i is the area of Section i of the nasal tract. Superscript l and r indicate the left and right nasal passages. The results obtained from (2) and (4) for four subjects are plotted in Figure 10. The results show that both of the shape and area asymmetries vary from one subject to the other. Subject 2 shows less asymmetry than the other subjects, with a maximum asymmetry coefficient of area function is about 0.2. For the other subjects, the maximum asymmetry coefficient is about 0.3.

C. Measurement of the paranasal cavities

There are many airy sinuses called "the paranasal cavities" around the nasal cavity bilaterally, which should affect the acoustic properties of the nasal tract to some extent. The paranasal cavities consist of four different sinuses; the sphenoidal sinus (S. S.), the maxillary sinus (M. S.), the frontal sinus (F. S.) and the ethomoidal sinus (E. S.). Among the four kinds of sinuses, the acoustic property of the ethomoidal sinus is hard to describe by a lumped parameter because it consists of many small sinuses. Fortunately, it does not affect the acoustic properties of the nasal tract at frequencies below 3k Hz (Takeuchi, et al., 1971). Therefore, we focus on the remaining sinuses. Area functions of the paranasal cavities are plotted in Figure 11 for Subject 1, and the numerical data are listed in Table II for the four subjects.

Among the three paranasal cavities, the maxillary sinus is the largest in volume, and the frontal sinus is the smallest. Their individual differences, where C. V.s vary from 18.9% to 42.6%, are greater than that of the main passages. There is strong asymmetry between the left and right sides of the paranasal cavities. Acoustically, each cavity can behave as a Helmholtz resonator which contributes to the formation of the single pole-zero pair in the transfer function of the nasal tract. In previous research, the sinuses were assumed to be symmetrical, with left and right sinus pairs of contributing one pole-zero pair only. But due to the asymmetry between the left and right sides, each pair of the sinuses can produce at least two pole-zero pairs.

To describe the acoustic characteristics of these sinuses, it is necessary to perform further measurements of the sinus ostium besides their volumes. For this reason, we treated the nasal tract with the nasal decongestant before the MRI scan to clearly observe the ostiums. An example of the maxillary sinuses with the treatment is shown in Figure 12 for Subject 4. For this subject, the left and right ostiums of the maxillary sinus are located at different positions in the

anterior-posterior axis, and have different sizes in length and in radius. Morphological data of the maxillary and sphenoidal sinuses are listed in Table III, where it was not possible to measure the ostiums of the frontal sinus.

In order to confirm the validity of our data, we compared our results with anatomical data. Masuda (1992) measured 44 maxillary ostiums of skulls, and reported the radii of the ostiums were from 0.094 cm to 0.366 cm, and their average radius was 0.222 cm. The lengths of the ostiums were from 0.11 cm to 0.64 cm, and their average value was 0.25 cm. Our measurements for the maxillary sinus ostium are close to the average value though nasal mucosa may make ostiums longer and narrower to some extent.

D. Cross-sectional area of the vocal tract for nasal consonants

In Experiment 2, a series of MRI slices of the vocal tract were taken from five subjects, while they sustained a posture of nasal consonant production during MRI scanning. Based on the MRI data, a series of axial section slices were obtained by slicing a reconstructed 3D image with the method described in Section 3.2. While measuring cross-sectional areas in the anterior portion of the oral cavity for /m/, we had a difficulty in distinguishing the teeth from the airway, because the enamel has the same low level in brightness as the airway does in MRI images, where they are lack of imageable H^+. To avoid the error of counting the volume occupied by the teeth in the airspace, we measured the cross-sectional areas in sustained pronunciation of /m/, then measured teeth area in the same planes from a reconstructed image acquired with a non-phonating rest posture, where a clear boundary of the teeth was visible from their contact with surrounding tissue. Approximate cross-sectional areas of the anterior portion of the oral tract were obtained by subtracting teeth volume from the image obtained during phonation. The area functions of the vocal tract of /m/ of /ma/ and /n/ of /na/ are shown in Figure 13 for Subject 4.

To compare calculated transfer function with real speech sounds, we recorded speech signals of /m/ and /n/ soon after taking the MRI slices for the subject. Speech sound was recorded in an anechoic room where the subject lay on the floor in the supine position and uttered nasal consonants, as close to the same configuration of articulatory organs used during MRI scanning as possible. The sound signals were passed through a low-pass-filter of 5.7k Hz, and was sampled and converted at 12k Hz and 16 bits.

IV. ACOUSTIC ANALYSIS

A. Effect of asymmetry of the left and right nasal passages

It has been suggested that asymmetry of the nasal tract should cause an extra pole-zero pair (Fujimura, & Lindqvst, 1964, Lindqvst-Gauffin, & Sundberg, 1976). However, such asymmetry has not been confirmed by real morphological data of the nasal tract. In this section, we investigate the effect of nasal passage asymmetry on the transfer function of the nasal tract.

We begin by calculating and comparing transfer functions of the nasal tract in single-tube and dual-tube cases. From the measured data, it is known that the nasal tract has a complicated shape, which may affect sound wave propagation inside the nasal tract to some extent. Intuitively, the sectional shape of the nasal tract can be treated as a simple geometrical figure like an ellipse so that we can approximate the three-dimension shape of the nasal tract. In the elliptic case, the ratio of long axis to short axis is more than 20 in the middle portion for four subjects. A typical value in the middle portion is about 5.0 cm in long axis, and 0.25 cm in short axis. Thus, the tube is larger in width than in length for the meddle portion. Sound wave propagates in such a tube not only in the axial-dimension but also in the wide-dimension, so that it should be considered at least in axial and wide dimensions. As a rough approximation, however, we consider the sound wave propagating

along the axial-dimension of the nasal tract only here, and use two transmission line models to calculate transfer function of the nasal tract. One is a single-tube model in which cross-sectional area is the sum of the left and right nasal passage areas. The other is a dual-tube model where the left and right nasal passages are considered separately. In those models, the impedance of the sound source is assumed infinite, i.e., the velopharyngeal port is closed, and the radiation impedance at the nostrils is zero. The calculated transfer functions of the nasal tract from the velopharyngeal port to the nostrils are plotted in Figure 14 for four subjects. Pole-zero pairs appear at the transfer function calculated with the dual-tube model for Subject 1, 3, and 4 as shown in Figure 14 (b), and they fall in the 2k Hz to 2.5k Hz range. Of course, no pole-zero appears at the transfer function from the single-tube model shown in Figure 14 (a).

In order to clarify the effects of asymmetry, transfer functions from the velopharyngeal port to the left nostril and undamped pole-zero patterns at the bifurcation of two nasal passages are shown in Figure 15 for Subject 3 and Subject 2. For Subject 3, the transfer function has two pole-zero pairs in frequency range below 5k Hz. For Subject 2, however, only one pole-zero pair appears at that range in his transfer function. To investigate the difference, pole-zero patterns are plotted in Figure 15 (b) and (c). According to the theory of a transmission line model with a branch, the acoustic effect of the branch, the right nasal passage, can be described by a series of admittances that are driving point impedances from the bifurcation to right passage(Yr), to left passage(Yl) and to velopharyngeal port(Yv). Zeros occur in the transfer function at frequencies where admittance Yr is infinite, and poles occur in the transfer function at frequencies where the sum of admittance Yr, Yl and Yv equals zero. When the left nasal passage acts as a branch, the corresponding pattern is also true. The pole-zero pattern shows that two pole-zero pairs occur at about 1860 Hz and 4350 Hz for Subject 3, where the admittance Yr is infinite. Similarly, two pole-zero pairs

occur at about 2460 Hz and 4670 Hz for Subject 2. However, the pole and zero of pole-zero pair at 2460 Hz for Subject 2 are so close that they counteract each other. Thus, the pole-zero pair that is caused by the asymmetry of two nasal passages does not appear at that frequency range. This is consistent with the asymmetry coefficient analysis, where Subject 2 has a slighter asymmetry than other subjects.

The results show that the first resonance frequency of the nasal tract does not change much between the two models. The first resonance frequency was located in 549-712 Hz with the single-tube model for four subjects, and located in 543-707 Hz with the dual-tube model. They varied about 6 Hz only from the one model to the other. The first nasal resonance frequency of three subjects is higher than 620 Hz. This is much higher than the 450 Hz that is a typical value for the first nasal formant estimated from real speech (Maeda, 1982).

B. Frequency characteristics of the nasal tract with paranasal sinuses

To investigate the acoustic properties of the nasal tract in further detail, we calculate the transfer function of the vocal tract from the area function for nasal consonants obtained in Section 4.4, and compare it to real speech spectra. Figure 16 shows a calculated transfer function of /n/ in Curve (a) obtained from the dual-tube model, where the vocal tract wall is treated as a yielding wall with a finite impedance (Ishizaka, French, and Flanagan, 1975). A spectrum of real speech sound for /n/ is plotted in Curve (b) which was obtained by cepstram analysis of the recorded speech signal. Though a lot of peaks and dips appear in the spectrum of real speech signal below 2k Hz, only two peaks and one dip appear in the calculation, where the dip is a zero caused by the oral cavity. This suggests that the complicated structure of the nasal cavity such as paranasal cavities should be taken into account during modeling the nasal cavity. Taking the paranasal sinus as a Helmholtz resonator, we

adopt the paranasal sinus data from the same subject into the vocal tract model. Thus, several pole-zero pairs should appear in transfer function whose frequencies can be predicted by Formula (5):

$$f = \frac{c}{2\pi}\sqrt{\frac{S}{V \bullet L}} \qquad (5)$$

where c is the sound velocity (approximately 35000 cm/s), and V is a volume of paranasal cavity in cm^3. S is the cross-sectional area of the ostium in cm^2, and L is its length in cm. Resonance frequencies of paranasal cavities are listed in Table IV, where their sizes are from Table III. From Table IV, it is known that due to the asymmetry the same kind of sinus can cause two pole-zero pairs with different central frequencies.

After the data of the paranasal cavities were included in the dual-tube model, the first resonance frequency of the nasal tract varied from 666 Hz to 426 Hz for the subject. It is close to the value of 450 Hz estimated from real speech (Maeda, 1982). The transfer function, which was calculated from the dual-tube model with the paranasal sinuses, is plotted in Figure 16 as Curve (c). In the calculation, four dips appear below 2k Hz in the transfer function. One of them is caused by the oral cavity at 1550 Hz, which is at the same frequency as that in Curve (a). The others are caused by the paranasal sinuses, where two zeros located at frequencies of 654 Hz and 678 Hz caused by the left and right sides of the maxillary sinus have merged into one dip located at 677 Hz in the transfer function. The calculated result has a similar pole-zero pattern below 2k Hz to that obtained for the real speech signal after the sinuses are taken into account, though we can not exclude the possibility that other factors besides the sinuses, such as sound source, caused the dips in the real speech signal. The result suggests that it is necessary to adopt the paranasal cavities into a model of the nasal cavity for describing its acoustic characteristics.

V. CONCLUSION

In this experiment, the nasal cavity and the paranasal cavities were measured by using MRI equipment. Results showed that the volume of the nasal cavity varies widely from one subject to the other even though the length changes little. When the nasal tract was morphologically divided into anterior, middle and posterior portions, results showed that the middle portion had the greatest individual differences.

A new series of slices were obtained from reconstructed 3D images, where the new slices were perpendicular to the midline of the vocal tract. The cross-sectional area and circumference of the airway were measured from these new slices. We obtained significantly different results from previously published data. We were able to reproduce the earlier results by employing a vasoconstrictor agent, showing that the primary source for the difference is the volume of the nasal mucosa. Because our nasal area function incorporates the mucosa, it provides a more realistic model of the nasal tract.

The cross-sectional area and circumference of the nasal cavity measured in this experiment offer useful information about the complexity of nasal tract shape. Using area and circumference data, the cross-sectional shape of the nasal tract can be approximated by a simple geometrical figure such as an ellipse. After the approximation, the shape of the middle nasal tract can typically be represented as an elliptic tube with long axis of 5 cm and short axis of 0.25 cm. It is not likely that sound wave propagates through the tube as a plane wave, because the size of the middle portion is greater in width than in length. Our data can be better exploited by other methods such as the finite element method, to simulate the sound wave propagation inside the nasal cavity. We also proposed a shape factor for the nasal tract, which is of the order of 1 for the posterior portion, 4 for the middle portion, and 2 for the anterior portion. Those portions are about 4.5 cm, 3.5 cm and 3.6 cm long, respectively.

Volume of the paranasal cavities and a part of their ostiums were measured in this experiment. The volume compares well with the previous anatomical measurement (Ref. Masuda, 1992). The results of plane wave acoustic calculations suggest that the effect of the paranasal cavities can not be neglected because those sinuses play an important role in shaping the frequency characteristics of the nasal cavity. Our data is sufficiently reliable to be used for building an acoustical model of the nasal cavity by comparing the calculated result to real speech.

It is confirmed by our measured data that left and right nasal passages are often asymmetric, and the asymmetry usually causes extra pole-zero pairs in the transfer function of the nasal tract. The asymmetry of the paranasal sinuses also affects the transfer function. These results suggest that asymmetry of the nasal cavity including the nasal passages and paranasal cavities must be considered in any accurate acoustic model of the nasal cavity.

ACKNOWLEDGMENTS

The authors would like to express their appreciation to Dr. Yasuhiro Shimada and his assistant for their helpful work in acquiring MRI images, and our colleagues for their discussions in data analysis. The authors also would like to thank Dr. Shiji Maeda for valuable comments and discussions.

Baer, T., Gore, J. C., Gracco, L. C. and Nye, P.W. (1991). "Analysis of vocal tract shape and dimensions using magnetic resonance imaging: vowels," J. Acoust. Soc. Am., 90, 2, 799-828.

Dang, J., Honda, K. and Suzuki H. (1993). "Morphological measurement of the nasal cavity and analysis resonance characteristics" Technical Report of IEICE, SP92-137, 1-8. (in Japanese)

Fant, G. (1960). Acoustic theory of speech production, (MOTON), p.139 (2nd ed., 1970).

Fant, G. (1980). "The relations between area functions and the acoustic signals," Phonetica, 37, 55-86.
Fujimura, O. and Lindqvst, J. (1964). "The sinewave response of the nasal tract," Q, prog. Status Rep., R. Inst. Technal., Stockh. 1, 5-10.
Fujimura, O. and Lindqvst, J. (1971). "Sweep-tone measurement of vocal-tract characteristics," J. Acoust. Soc. Am. 49, 2, 541-558.
House, A. S. and Stevens, K. N. (1956). "Analog studies of the nasalization of vowels," J. Speech and Hearing Disorders, 21, 218-232.
Ishizaka, K, French, J. C. and Flanagan, J. L. (1975). "Direct determination of vocal tract wall impedance," IEEE Trans. Acoust. Speech Signal Process. ASSP-23, 370-373.
Lindqvst-Gauffin, J, and Sundberg, J. (1976). "Acoustic properties of the nasal tract," Phonetica, 33, 161-168.
Maeda, S.(1982). "The role of the sinus cavities in the production of nasal vowels," in Proc. IEEEE int. Conf. ASSP, 2, 911- 914.
Masuda, S. (1992) "Role of the maxillary sinus as a resonant cavity," J. Otolaryngology Soc. Jpn, 95-70. (in Japanese).
Moor, C. A. (1992). "The correspondence of vocal tract resonance with volumes obtained from magnetic resonance images," J. Speech and Hearing Res., 35, 1009-1023.
Takeuchi, S., Kasuya, H. and Kido, K. (1977). "A study on the effects of nasal and paranasal cavities on the spectra of nasal sounds," J. Acoust. Soc. Jpn. 33, 4 163-172. (in Japanese).

Table captions

Table I Morphological data of the nasal tract for four subjects.

Table II Morphological data of the paranasal cavities (Unit:cm^3.)

Table III Morphological data of the sphenoidal and maxillary sinuses of Subject 4.

Table IV Resonance frequency of the sphenoidal and maxillary sinuses of Subject 4.

Figure captions

Fig. 1 An example of coronal MRI slices for the nasal and paranasal cavities obtained from Sub. 1.

(a) An image at 3cm from the posterior wall of the pharynx.

(b) An image at 5.4cm from the posterior wall of the pharynx.

(c) An image at 8.4cm from the posterior wall of the pharynx.

Fig. 2 Sectional images of the nasal and paranasal cavities extracted from MRI slices shown in Fig.1.

(a) At 3cm from the posterior wall of the pharyngx.

(b) At 5.4cm from the posterior wall of the pharynx.

(c) At 8.4cm from the posterior wall of the pharynx.

Fig. 3 A projection of 3D image of the nasal and paranasal cavities reconstructed from coronal slices like those shown in Fig. 2.

Fig. 4 Sectional images sliced up from a reconstructed 3D image(Sub. 1).

(a) Images in sagittal planes by the midsagittal plane in 0.3cm intevals.

(b) Images in transverse planes through superior, middle and inferior meatus, respectively.

Fig. 5 Angles and position of the axial planes to measure cross-sectional area of the vocal tract for /m/.

Fig. 6 Measured cross-sectional area of the nasal passages.

Fig. 7 Cross-sectional area of the nasal tract of our data and previous data.

(a) The data by Fant (1960).

(b) Nasal tract treated without adrenaline for Sub. 2.

(c) Nasal tract treated with adrenaline for Sub. 2.

Fig. 8 Measured cross-sectional circumference of the nasal passages.

Fig. 9 Shape factor of the nasal tract for four subjects.

Fig. 10 Asymmetry of left and right passages of the nasal tract.

Fig. 11 Area function of the paranasal cavities in coronal planes from posterior wall of the pharynx to the nostrils for Sub.1.

Fig. 12 Left and right ostiums of the maxillary sinus for Sub. 4. (pointed at by black arrows).

(a) Left ostium located at 6.3cm from the posterior wall of the pharynx.

(b) Right ostium located at 6cm from the posterior wall of the pharynx.

Fig. 13 Area functions of /m/ and /n/ from the glottis to the lips or the nostrils, one section is 0.3cm long).

Fig. 14 Transfer function of the nasal tract by a single-tube model and a dual-tube models (The arrows point at pole-zeros).

(a) Transfer function of the nasal tract by a single-tube model.

(b) Transfer function of the nasal tract by a dual-tube model.

Fig. 15 Transfer functions from the velopharyngeal port to the left nostril and their undamped pole-zero patterns (Yv,Yl and Yr are admitances from the branch to the velopharyngeal port, left and right nostrils).

(a) Transfer functions for Sub. 3 and Sub. 2, where right nasal passage acts as a branch.

(b) Undamped pole-zero pattern at the branch for Sub. 3.

(c) Undamped pole-zero pattern at the branch for Sub. 2.

Fig. 16 Transfer function of the vocal tract from the glottis to the nostrils for /n/ (Arrows point at pole-zeros or dips).

(a) Calculation in a dual-tube model without sinuses.

(b) Spectrum obtained from real speech signal by cepstram analysis.

(c) Calculation in a dual-tube model with sinuses.

Table I Morphological data of the nasal tract for four subjects.

	Sub.1	Sub.2	Sub.3	Sub.4	Avg.	Std.	C.V %
Total length	11.7	11.7	11.7	11.4	11.6	0.13	1.1
Total volume	26.5	20.4	39.7	15.4	25.5	9.09	35.7
Length of P. P.	3.6	4.2	3.6	4.2	3.9	0.30	7.7
Volume of P. P.	10.6	6.4	7.4	6.7	7.8	1.67	21.5
Surface of P. P.	27.1	21.8	19.8	21.8	22.6	2.71	12.0
Length of M. P.	4.2	4.2	4.8	4.2	4.4	0.26	6.0
Volume of M. P.	11.0	9.2	16.7	5.7	10.7	3.98	37.4
Surface of M. P.	92.0	99.6	105.5	57.6	88.7	18.57	20.9
Length of A. P.	3.9	3.3	3.3	3.0	3.4	0.33	9.7
Volume of A. P.	5.0	4.8	5.6	3.1	4.6	0.93	20.1
Surface of A. P.	36.2	28.9	30.9	20.7	29.2	5.57	19.1

*P. P., M. P. and A. P. represent posterior, meddle and anterior portions of the nasal tract respectively.

**Units are cm for length, cm^2 for area and cm^3 for volume.

Table II Morphological data of the paranasal cavities (Unit:cm^3).

	Sub.1	Sub.2	Sub.3	Sub.4	Avg.	Std.	C.V %
Volume of S. S.(R)	9.0	12.1	7.6	8.4	9.0	1.70	18.9
Volume of S. S.(L)	14.2	5.2	10.2	5.7	8.9	3.66	41.2
Volume of M. S.(R)	19.9	16.5	21.8	11.0	17.3	4.10	23.7
Volume of M. S.(L)	16.8	16.1	20.3	9.9	15.7	3.75	23.9
Volume of F. S.(R)	2.2	3.1	4.1	1.1	2.6	1.11	42.6
Volume of F. S.(L)	3.1	4.9	4.8	1.6	3.6	1.36	37.7

*L and R represent the left and right sides respectively.

**S. S.:The Sphenoidal Sinus. M. S.:The Maxillary Sinus. F. S.:The Frontal Sinus.

Table III Morphological data of the sphenoidal and maxillary sinuses of Subject 4.

	Volume(cm^3)	Radius(cm)	Length(cm)	Position(cm)
Right of S. S.	8.36	0.098	0.391	4.2
Left of S. S.	5.74	0.130	0.293	4.2
Right of M. S.	11.0	0.154	0.451	6.0
Left of M. S.	9.92	0.128	0.375	6.3

*S. S.: The Sphenoidal Sinus. M. S.: The Maxillary Sinus.

J. Acoust. Soc. Am.
J. Dang, K. Honda and H. Suzuki: Analysis of the nasal and the paranasal cavities.

Table IV Resonance frequency of the sphenoidal and maxillary sinuses of Subject 4.

	Right of S. S	Left of S. S.	Right of M. S.	Left of M. S.
Frequency(Hz)	534	989	678	654

*S. S.: The Sphenoidal Sinus. M. S.: The Maxillary Sinus.

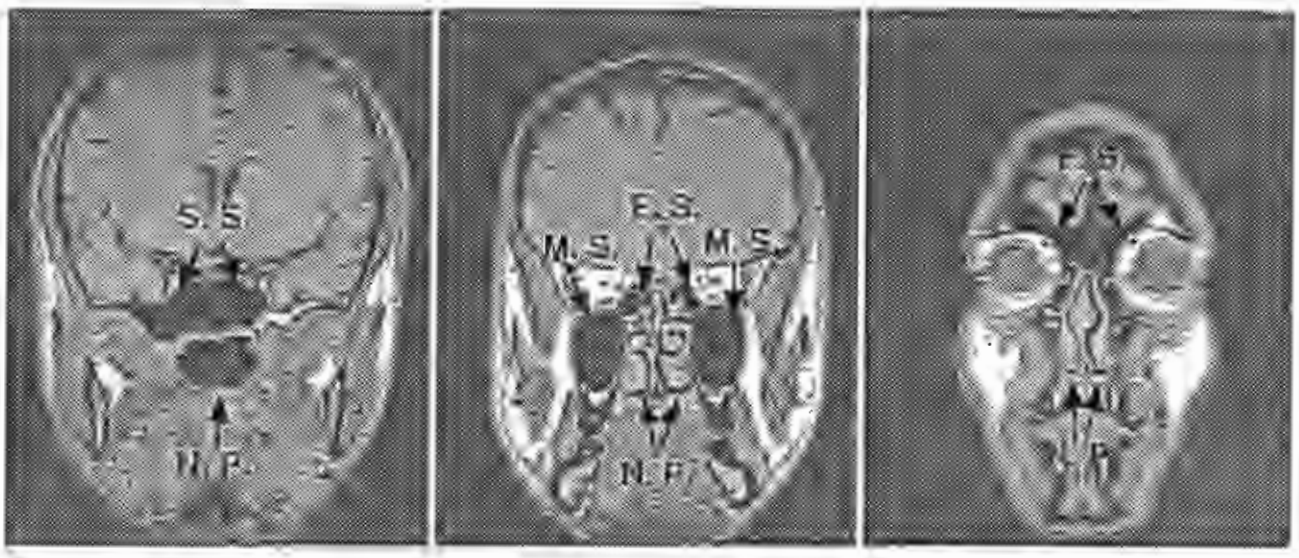

(a) (b) (c)

N. P.: Nasal Passage. S. S.: The Sphenoidal Sinus.

E. S.: The Ethomoidal Sinus. M. S.: The Maxillary Sinus. F. S.: The Frontal Sinus.

Fig. 1 An example of coronal MRI slices for the nasal and paranasal cavities obtained from Sub. 1.
(a) An image at 3cm from the posterior wall of the pharynx.
(b) An image at 5.4cm from the posterior wall of the pharynx.
(c) An image at 8.4cm from the posterior wall of the pharynx.

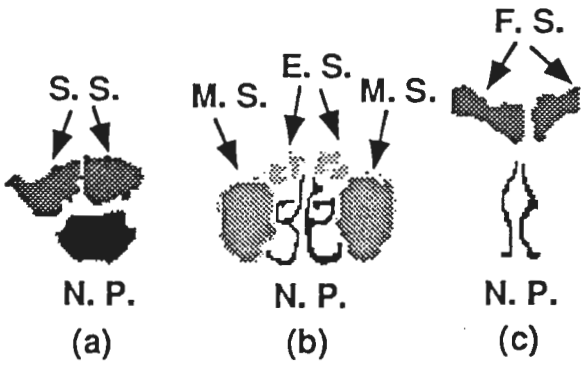

N. P.: Nasal Passage.
S. S.: The Sphenoidal Sinus.
M. S.: The Maxillary Sinus.
E. S.: The Ethomoidal Sinus.
F. S.: The Frontal Sinus.

Fig. 2 Sectional images of the nasal and paranasal cavities extracted from MRI slices shown in Fig.1.
(a) At 3cm from the posterior wall of the pharyngx.
(b) At 5.4cm from the posterior wall of the pharynx.
(c) At 8.4cm from the posterior wall of the pharynx.

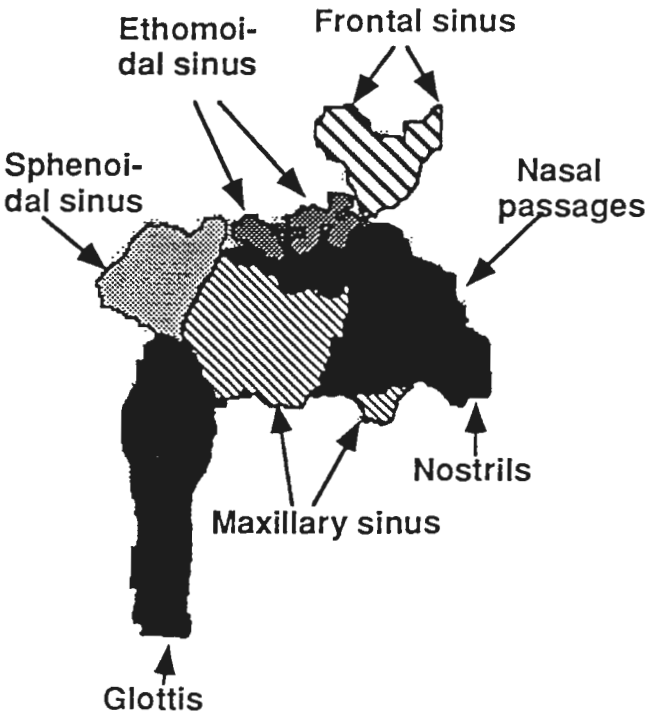

Fig. 3 A projection of 3D image of the nasal and paranasal cavities reconstructed from coronal slices like those shown in Fig. 2.

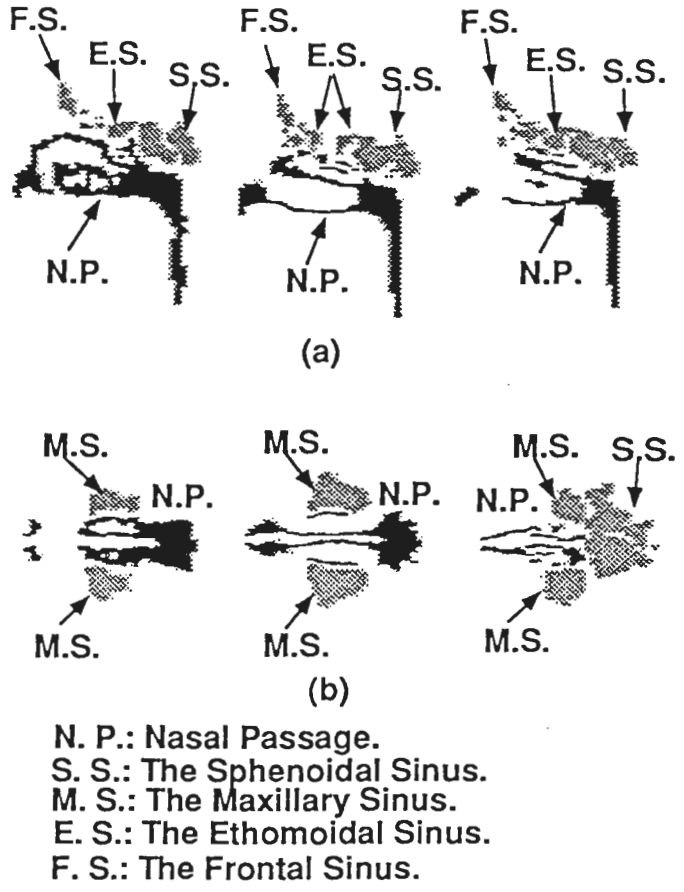

Fig.4 Sectional images sliced up from a reconstructed 3D image(Sub. 1).
(a) Images in sagittal planes by the midsagittal plane in 0.3cm intevals.
(b) Images in transverse planes through superior, middle and inferior meatus, respectively.

J. Acoust. Soc. Am.
J. Dang, K. Honda and H. Suzuki: Analysis of the nasal and the paranasal cavities.

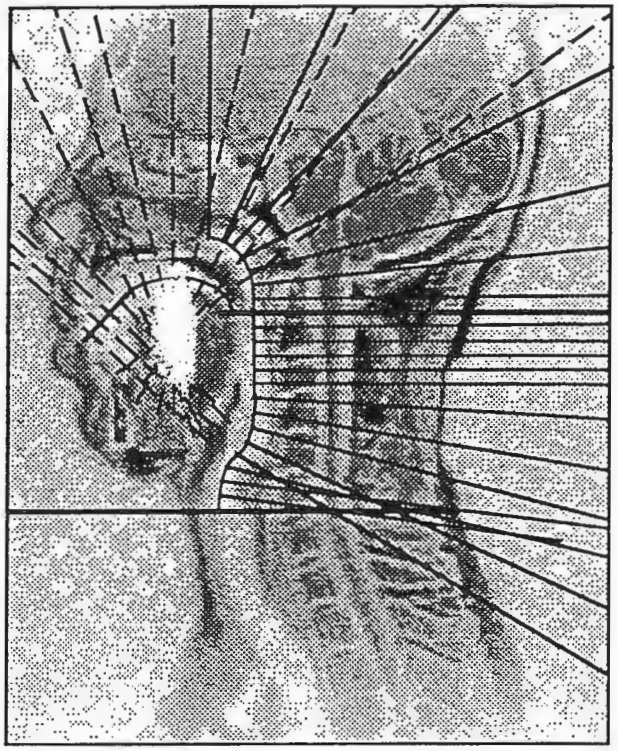

— : For the pharyngeal and posterior portion of the nasal cavities.

— —: For the oral cavity. ——: For boundaries.

Fig. 5 Angles and position of the axial planes to measure cross-sectional area of the vocal tract for /m/.

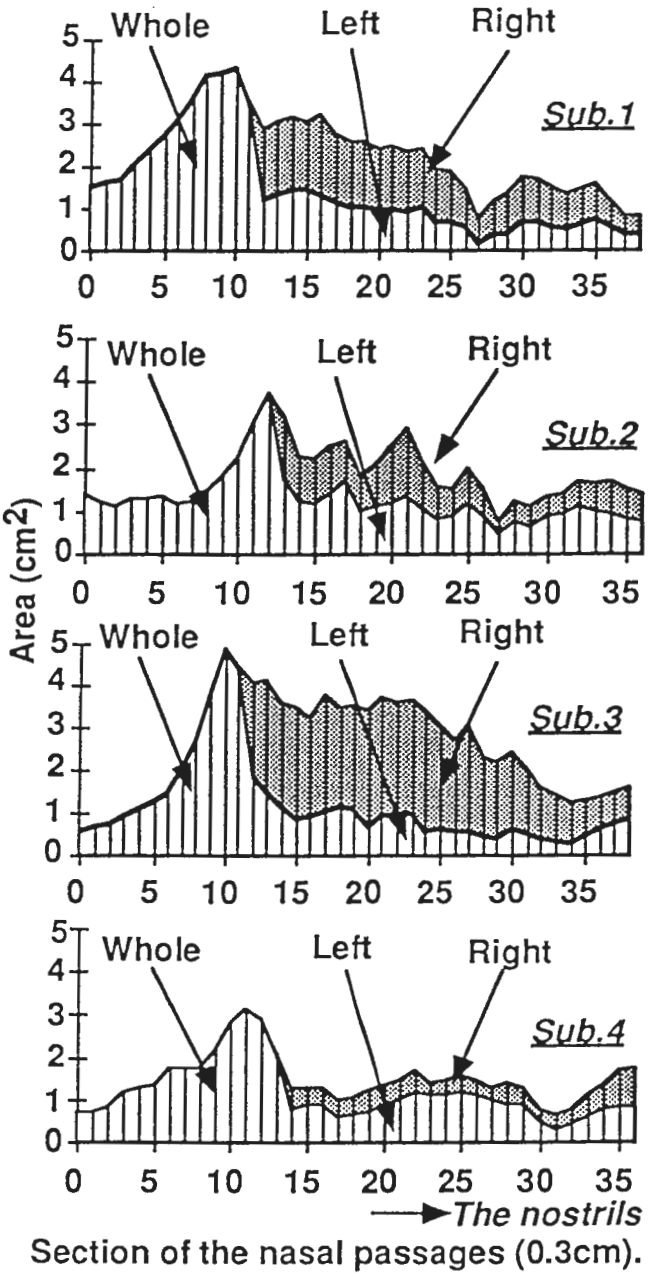

Fig. 6 Measured cross-sectional area of the nasal passages.

J. Acoust. Soc. Am.
J. Dang, K. Honda and H. Suzuki: Analysis of the nasal and the paranasal cavities.

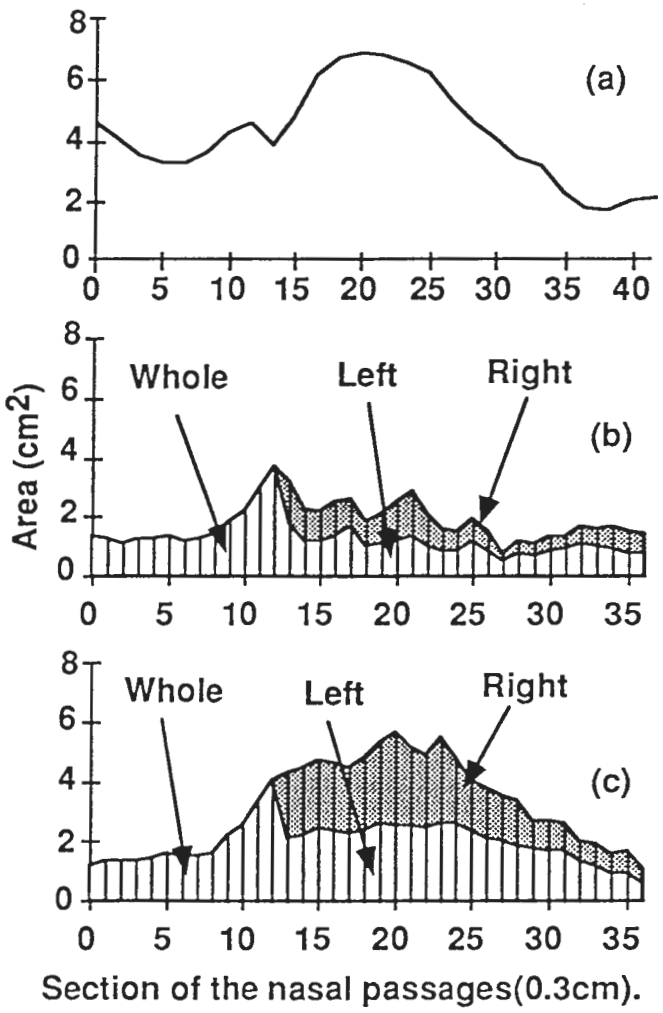

Fig. 7 Cross-sectional area of the nasal tract of previous data and our data.
(a) The data by Fant (1960).
(b) Nasal tract treated without adrenaline for Sub. 2.
(c) Nasal tract treated with adrenaline for Sub. 2.

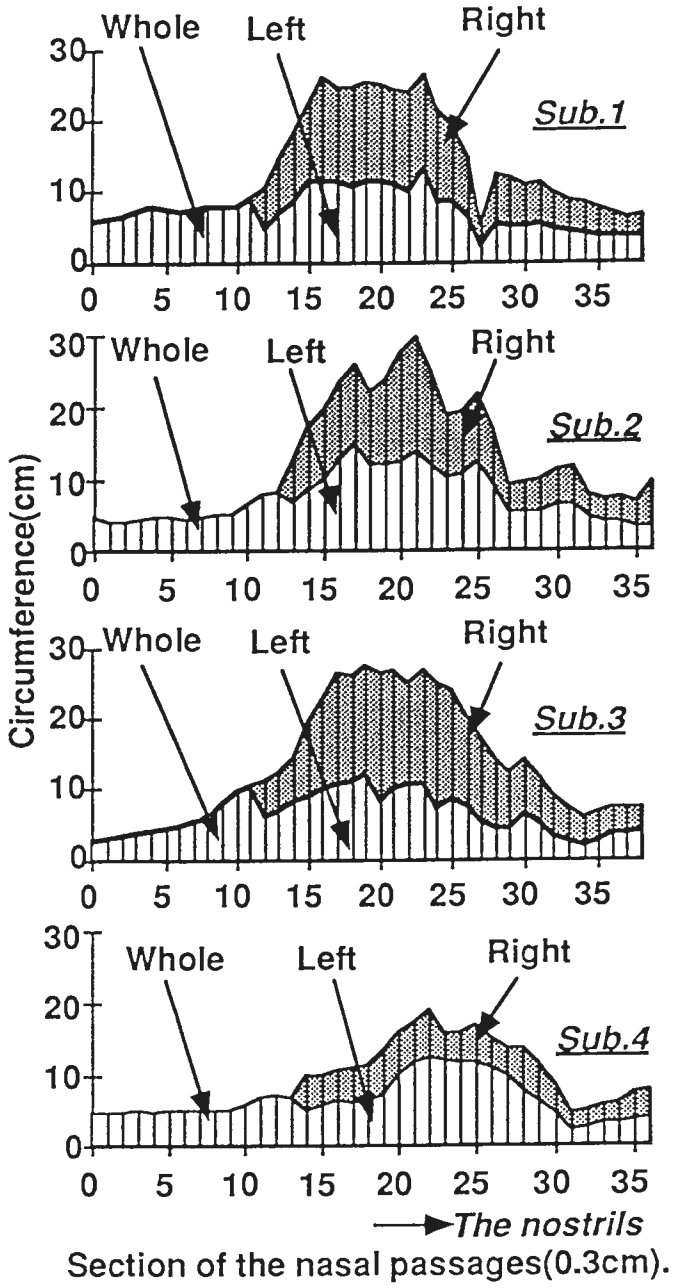

Fig. 8 Measured cross-sectional circumference of the nasal passages.

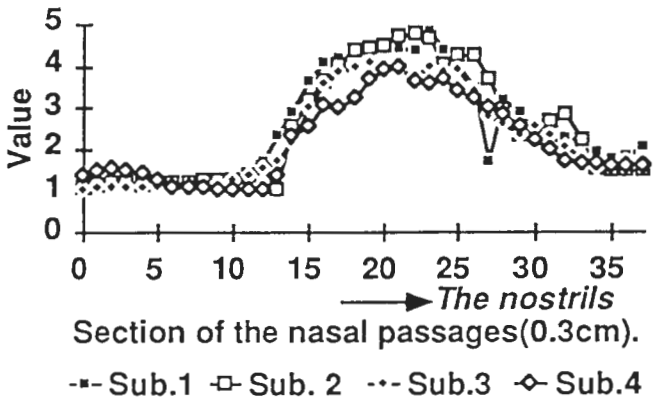

Fig. 9 Shape factor of the nasal tract for four subjects.

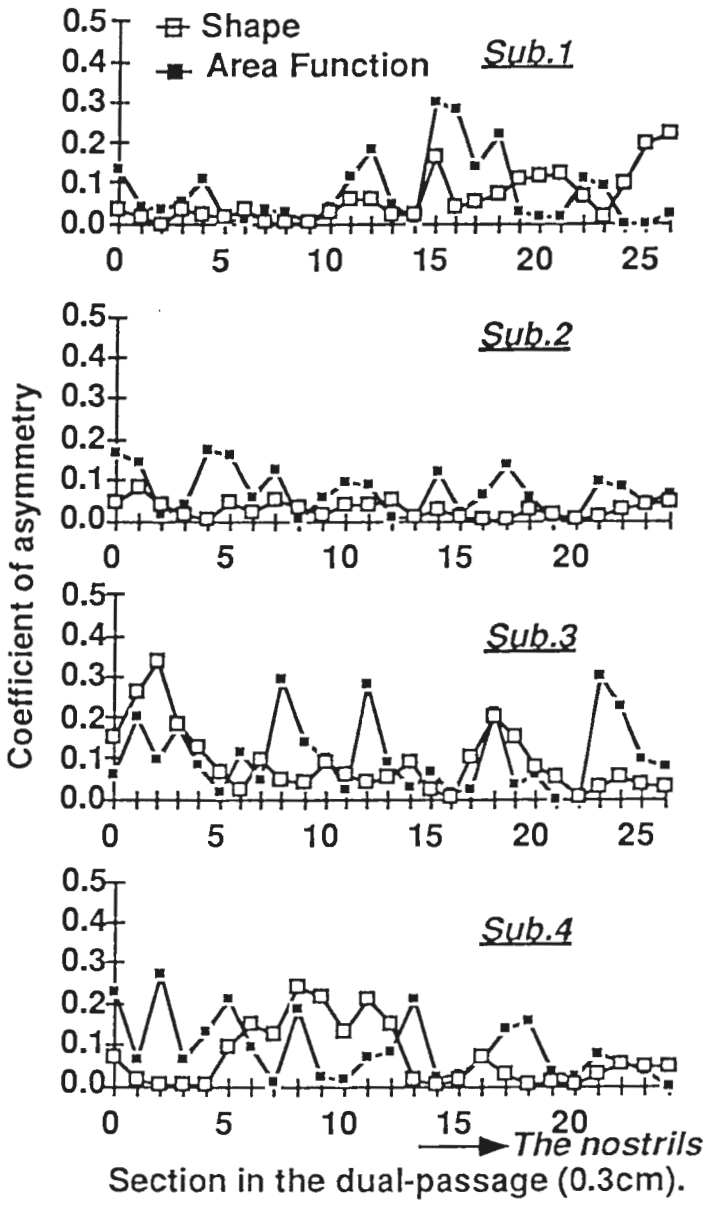

Fig. 10 Asymmetry of left and right passages of the nasal tract.

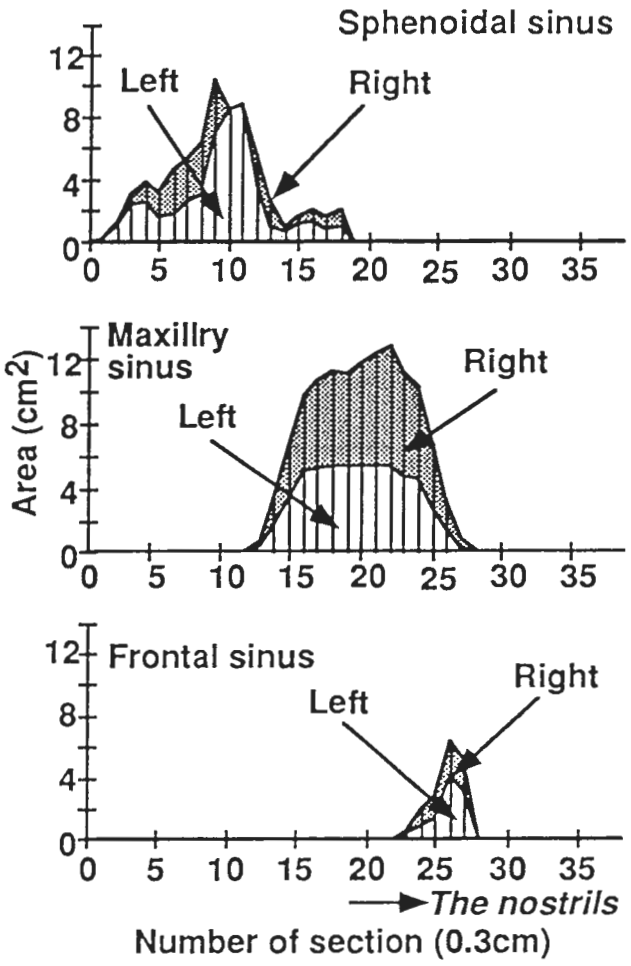

Fig.11 Area function of the paranasal cavities in coronal planes from posterior wall of the pharynx to the nostrils for Sub.1.

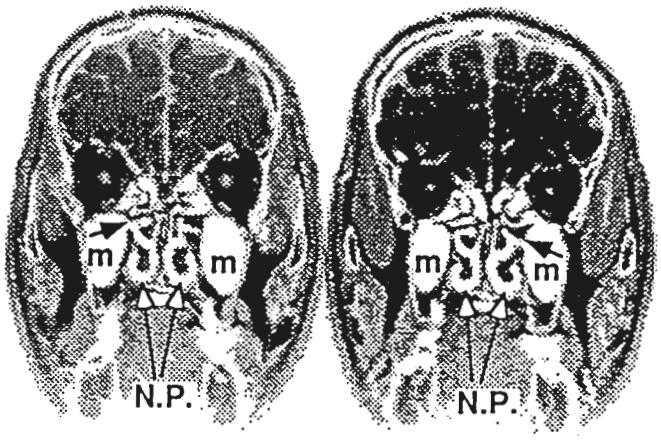

(a) (b)

N.P.: Nasal passages. m: The maxillary sinus.

Fig. 12 Left and right ostiums of the maxillary sinus for Sub. 4.
(pointed at by black arrows).
(a) Left ostium located at 6.3cm from the posterior wall of the pharynx.
(b) Right ostium located at 6cm from the posterior wall of the pharynx.

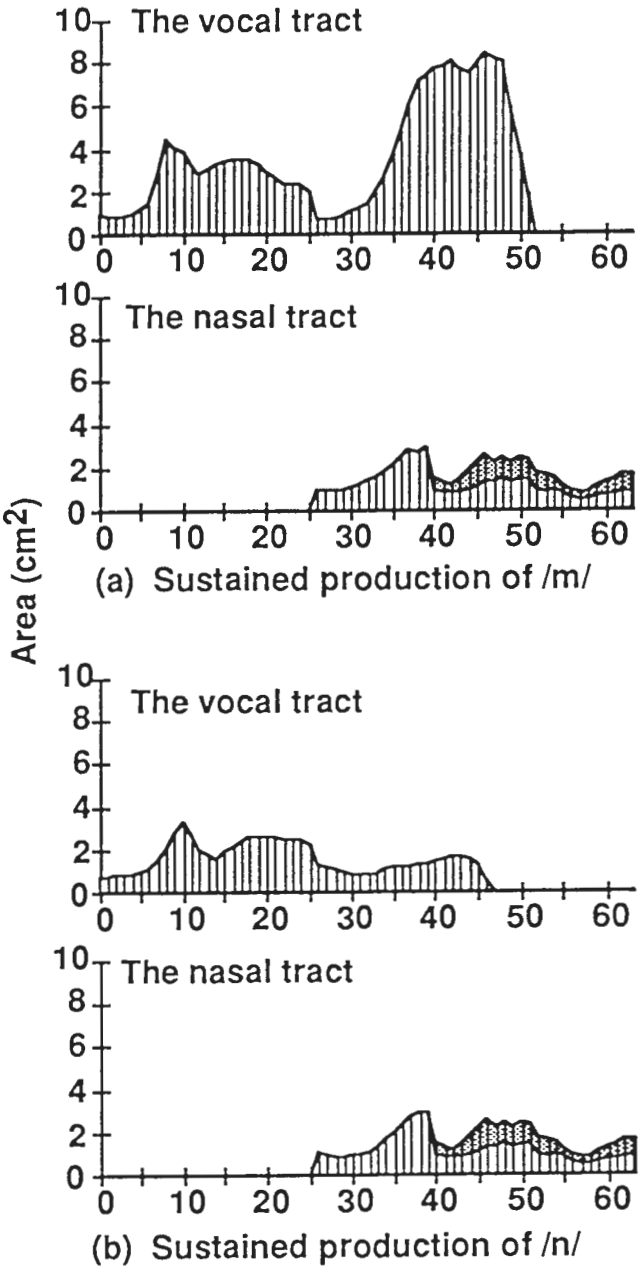

Fig. 13 Area functions of /m/ and /n/ from the glottis to the lips or the nostrils, one section is 0.3cm long).

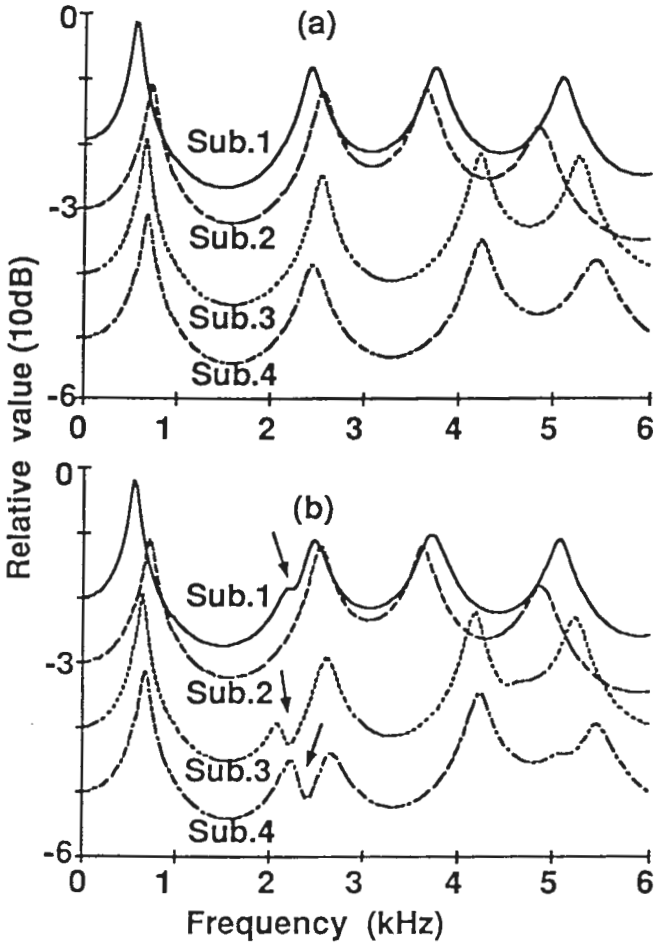

Fig. 14 Transfer function of the nasal tract by a single-tube model and a dual-tube models (The arrows point at pole-zeros).
(a) Transfer function of the nasal tract by a single-tube model.
(b) Transfer function of the nasal tract by a dual-tube model.

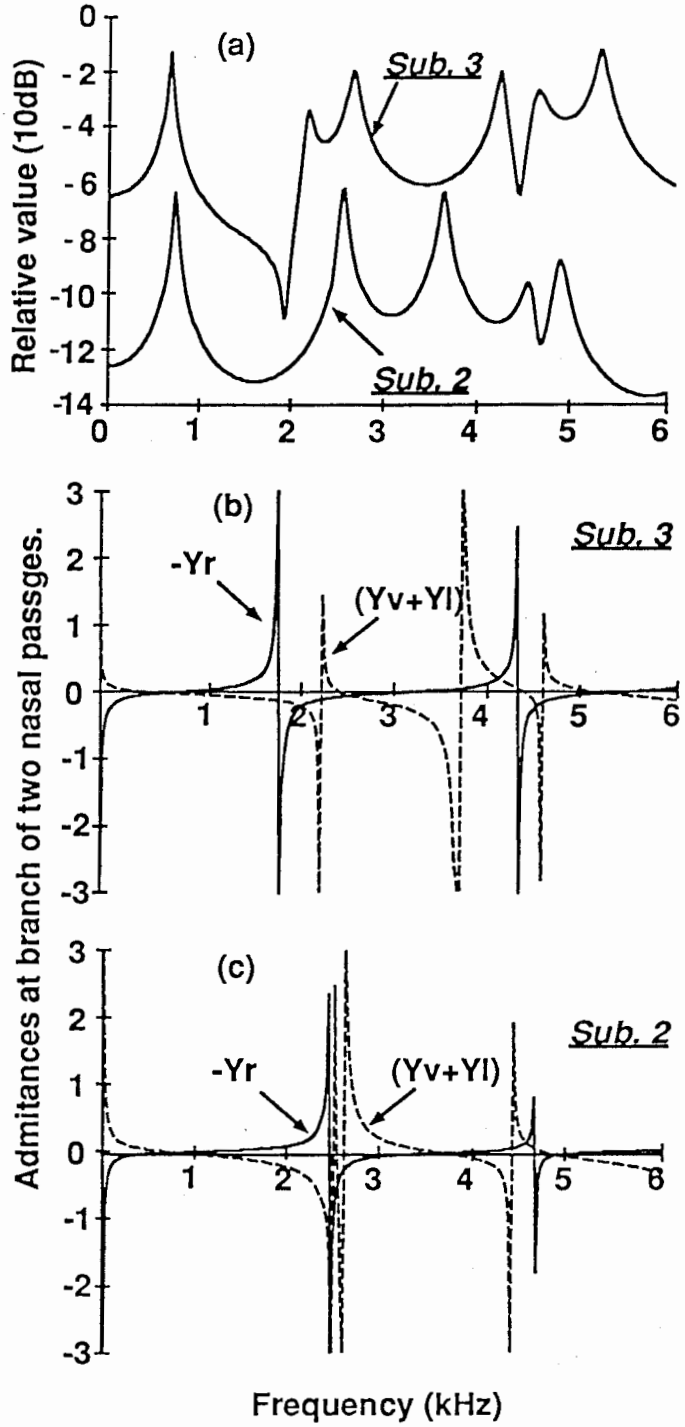

Fig. 15 Transfer functions from the velopharyngeal port to the left nostril and their undamped pole-zero patterns (Yv,Yl and Yr are admitances from the branch to the velopharyngeal port, left and right nostrils).
(a) Transfer functions for Sub. 3 and Sub. 2, where right nasal passage acts as a branch.
(b) Undamped pole-zore pattern at the branch for Sub. 3.
(c) Undamped pole-zore pattern at the branch for Sub. 2.

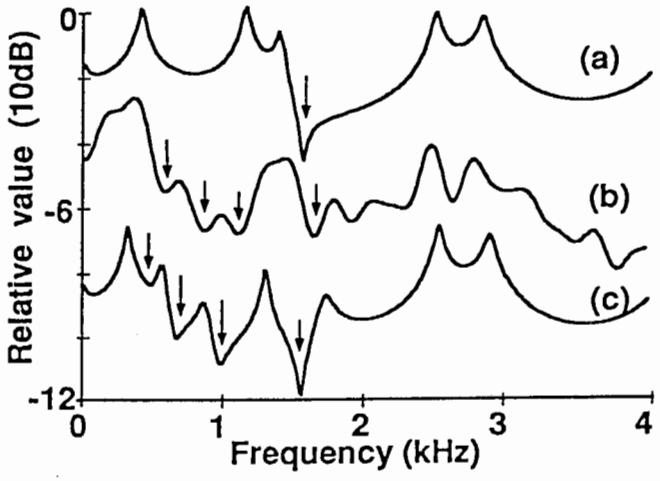

Fig. 16 Transfer function of the vocal tract from the glottis to the nostrils for /n/ (Arrows point at pole-zeros or dips).
(a) Calculation in a dual-tube model without sinuses.
(b) Spectrum obtained from real speech signal by cepstrum.
(c) Calculation in a dual-tube model with sinuses.

J. Acoust. Soc. Am.
J. Dang, K. Honda and H. Suzuki: Analysis of the nasal and the paranasal cavities.